Langmuir
Article
pubs.acs.org/Langmuir

Renewable Nanocomposite Layer-by-Layer Assembled Catalytic Interfaces for Biosensing Applications

Saroja Mantha,[†] Valber A. Pedrosa,[†,∥] Eric V. Olsen,[§] Virginia A. Davis,[‡] and Aleksandr L. Simonian*[,†]

[†]*Materials Research and Education Center,* [‡]*Department of Chemical Engineering, Auburn University, Auburn, Alabama 36849, United States, and* [§]*Clinical Research Laboratory, 81st Medical Group, Keesler AFB, Mississippi 39534, United States .* [∥]*Current address: Instituto de Biociências, Departamento de Química e Bioquímica, UNESP, Botucatu, SP, Brazil.*

Received August 24, 2010. Revised Manuscript Received October 22, 2010

A novel, easily renewable nanocomposite interface based on layer-by-layer (LbL) assembled cationic/anionic layers of carbon nanotubes customized with biopolymers is reported. A simple approach is proposed to fabricate a nanoscale structure composed of alternating layers of oxidized multiwalled carbon nanotubes upon which is immobilized either the cationic enzyme organophosphorus hydrolase (OPH; MWNT−OPH) or the anionic DNA (MWNT−DNA). The presence of carbon nanotubes with large surface area, high aspect ratio and excellent conductivity provides reliable immobilization of enzyme at the interface and promotes better electron transfer rates. The oxidized MWNTs were characterized by thermogravimetric analysis and Raman spectroscopy. Fourier transform infrared spectroscopy showed the surface functionalization of the MWNTs and successful immobilization of OPH on the MWNTs. Scanning electron microscopy images revealed that MWNTs were shortened during sonication and that LbL of the MWNT/biopolymer conjugates resulted in a continuous surface with a layered structure. The catalytic activity of the biopolymer layers was characterized using absorption spectroscopy and electrochemical analysis. Experimental results show that this approach yields an easily fabricated catalytic multilayer with well-defined structures and properties for biosensing applications whose interface can be reactivated via a simple procedure. In addition, this approach results in a biosensor with excellent sensitivity, a reliable calibration profile, and stable electrochemical response.

Introduction

An emerging group of hybrid materials derived from novel nanostructures and biological molecules interacting at the nanometer scale has recently attracted great attention. Layer-by-layer (LbL) assembly of these materials is a simple, robust, and inexpensive method for designing nanocomposite thin films with a high degree of control that may provide potentially powerful interfaces for multiple applications.[1−3] Nanomaterials modified with biological molecules offer an attractive combination of intrinsic physical and chemical properties for a wide range of applications including mimetic biominerals,[4] biomedicine, and sensors.[5−7] A wide variety of new nanoparticle/biomolecule based assemblies are used for advanced detection of proteins.[8] Currently, the development of bionanocomposite systems based on nanostructured hybrid organic−inorganic materials are one of the most actively pursued research areas.[9] The integration of carbon nanotubes (CNT) and biopolymers can offer interesting electrical, mechanical and optical properties.[10−12] The ability to enhance direct electron transfer in enzyme-catalyzed electrode reactions has led to considerable interest in CNT nanocomposites for a wide range of applications such as biofuel cells, optical devices, sensors,[13,14] and catalysts.[15−25] Additionally, carbon nanotubes not only facilitate electron transfer ability but also serve as a good scaffold for the immobilization of biomolecules in a variety of biosensing systems.[26−28] However the effective

*To whom correspondence should be addressed. E-mail: als@auburn.edu.

(1) Hitzky, E. R.; Darder, M.; Aranda, P. *J. Mater.Chem.* **2005**, *15*, 3650–3662.
(2) Kumar, A. S.; Swetha, P. *Langmuir* **2010**, *26*, 6874–6877.
(3) Dujardin, E.; Mann, S. *Adv. Mater.* **2002**, *14*, 775–788.
(4) Palin, E.; Liu, H.; Webster, T. J. *Nanotechnology* **2005**, *16*, 1828–1836.
(5) Geetha, S.; Rao, C. R. K.; Vijayan, M.; Trivedi, D. C. *Anal. Chim. Acta* **2006**, *568*, 119–125.
(6) Yan, J.; Pedrosa, V. A.; Simonian, A. L.; Revzin, A. *ACS Appl. Mater. Interfaces* **2010**, *2*, 748–755.
(7) Riccardi, C. D.; Yamanaka, H.; Josowicz, M.; Kowalik, J.; Mizaikoff, B.; Kranz, C. *Anal. Chem.* **2006**, *78*, 1139–1145.
(8) Wang, J. *Electroanalysis* **2007**, *19*, 769–776.
(9) Darder, M.; Blanco, M. L.; Aranda, P.; Leroux, F.; Hitzky, E. R. *Chem. Mater.* **2005**, *17*, 1969–1977.
(10) Liu, T. X.; Phang, I. Y.; Shen, L.; Chow, S. Y.; Zhang, W. D. *Macromolecules* **2004**, *37*, 7214–7222.
(11) Raravikar, N. R.; Schadler, L. S.; Zhao, Y. P.; Wei, B. Q.; Ajayan, P. M. *Chem. Mater.* **2005**, *17*, 974–983.
(12) Du, F. M.; Scogna, R. C.; Zhou, W.; Brand, S.; Fischer, J. E.; Winey, K. I. *Macromolecules* **2004**, *37*, 9048–9055.
(13) Kim, S. N.; Rusling, J. F.; Papadimitrakopolous, F. *Adv. Mater.* **2007**, *19*, 3214–3228.
(14) Rusling, J. F.; Yu, X.; Munge, B. S.; Kim, S. N.; Papadimitrakopoulos, F. *Engineering the Bioelectronic Interface*; Davis, J., Ed.; Royal Society of Chemistry: U. K., 2009; p 94.
(15) Chen, G. Z.; Shaffer, M. S. P.; Coleby, D.; Dixon, G.; Zhou, W. Z.; Fray, D. F.; Windle, A. H. *Adv. Mater.* **2000**, *12*, 522–526.
(16) Zhang, X. T.; Zhang, J.; Wang, R. M.; Zhu T, T.; Liu, Z. F. *ChemPhysChem* **2004**, *5*, 998–1002.
(17) Privman, V.; Pedrosa, V. A.; Melnikov, D.; Pita, M.; Simonian, A. L.; Katz, E. *Biosens. Bioelectron.* **2009**, *25*, 695–701.
(18) Frackowiak, E.; Khomenko, V.; Jurewicz, K.; Lota, K.; Beguin, F. *J. Power Sources* **2006**, *153*, 413–418.
(19) Callegari, A.; Cosnier, S.; Marcaccio, M.; Paolucci, D.; Paolucci, F.; Georgakilas, V.; Tagmatarchis, N.; Vázquez, E.; Prato, M. *J. Mater. Chem.* **2004**, *14*, 807–810.
(20) Katz, E.; Willner, I. *ChemPhysChem* **2004**, *5*, 1084–1104.
(21) Wang, J. *Electroanalysis* **2005**, *17*, 7–14.
(22) Lin, Y.; Taylor, S.; Li, H.; Fernando, K. A. S.; Qu, L.; Wang, W.; Gu, L.; Zhou, B.; Sun, Y. P. *J. Mater. Chem.* **2004**, *14*, 527–541.
(23) Allen, B.; Kichambare, P.; Star, A. *Adv. Mater.* **2007**, *19*, 1439–1451.
(24) Ghindilis, A. L.; Atanasov, P.; Wilkins, E. *Electroanalysis* **1997**, *9*, 661–674.
(25) Joshi, P. P.; Merchant, S. A.; Wang, Y.; Schmidtke, D. W. *Anal. Chem.* **2005**, *77*, 3183–3188.
(26) Chikkaveeraiah, B. V.; Bhirde, A.; Malhotra, R.; Vyomesh, P.; Silvio Gutkind, J.; Rusling, J. F. *Anal. Chem.* **2009**, *81*, 9129–9134.
(27) Lee, D.; Cui, T. H. *IEEE Sens. J.* **2009**, *9*, 449–456.
(28) Wang, Y. D.; Joshi, P. P.; Hobbs, K. L.; Johnson, M. B.; Schmidtke, D. W. *Langmuir* **2006**, *22*, 9776–9783.

utilization of CNTs in biosensing applications depends strongly on the viability and functional activity of immobilized bioplymers, as well as on the ability to prevent bundling and disperse the CNTs homogeneously throughout the matrix without destroying their structural integrity. Considerable research efforts have focused on the chemical functionalization of the CNTs with organic groups or polymers[29,30] for proper immobilization of biorecognition structures.[31,32] Chemical modifications, such as acid treatment, not only enable CNT dispersion in aqueous solutions but also facilitate uniform distribution and tight matrix connectivity in the construction of CNT-based materials. LbL assembly of well dispersed CNT is a powerful approach for providing nanoscale thickness and orientation control and the assembly of multiple layers with unique compositions and physical attributes. This method relies on the electrostatic interaction of oppositely charged layers, and has been utilized via alternate adsorption of oppositely charged polyions and biopolymers involving a variety of organic and inorganic substrate materials, including CNTs,[33,34] lysozyme,[35] proteins,[36] antigen,[37] DNA,[38] nanoparticles,[39] metallophthalocyanines,[40] and dendrimers.[41] The sandwich-like LbL structure provides a suitable microenvironment to retain the molecular activity of incorporated biopolymers. Recently, we demonstrated that the using the LbL approach for dispersions of CNTs and biopolymers results not only in strong mechanical properties due to the CNTS, but also retention of biopolymer functional properties such as the antimicrobial properties of lysozyme.[35]

The objective of this work was to design the hybrid catalytic interfaces based on the interaction of anionic/cationic biomolecular layers structured with MWNTs (Figure 1). The initial step requires assembling a supporting bilayer of oppositely charged MWNT−polyethyleneimine (PEI) and MWNT−DNA. This allows for further adsorption of a positively charged complex of MWNT−protein which adsorbs better on this cushioning support rather than adsorbing directly on a solid support. As an example we used here a complex of MWNT−OPH, a well-known enzyme capable of hydrolyzing variety of organophosphate neurotoxins.[42] The interface with MWNT−OPH on the top was utilized in monitoring the paraoxon hydrolysis reaction using UV−visible spectroscopy and amperometry, having in mind a demonstration of applicability of the nanocomposite multilayers to bioanalytical chemistry. Importantly, the sensor interface could be easily and reproducibly renewed. These novel renewable multilayers of biopolymer/CNT reflect their superior electrocatalytic characteristics, large specific surface area, long-term stability, and fast electron transfer. The optimization and advantages of the novel functional interfaces are reported in the following sections.

Experimental Section

Materials. MWNTs (purity 95%, length 1−5 μm, diameter 30 ± 10 nm) prepared by a chemical vapor deposition (CVD) process were purchased from Nanolabs; the as received material is referred to as raw MWNT. Organophosphorus hydrolase (OPH) was generously provided by James Wild and his research group (Texas A&M University). Paraoxon was obtained from ChemService, Inc. (West Chester, PA). DNA (lyophilized salmon sperm salt), *N*-hydroxysuccinimide (NHS), *N*-ethyl-*N*-(3-dimethylaminopropyl) carbodiimide hydrochloride (EDC), polyethyleneimine (PEI), 2-(*N*-morpholino)ethanesulfonic acid (MES), *N*-cyclohexyl-2-aminoethanesulfonic acid (CHES), and phosphate buffered saline (PBS) were all obtained from Sigma−Aldrich (St. Louis, MO). Water used for the preparation of aqueous solutions was from a Millipore Direct-Q Water system (resistivity, 18 MΩ cm^{-2}).

Instruments. The samples of raw MWNT and oxidized MWNT were analyzed by thermogravimetric analysis (TGA) using TGA Q500 (TA Instrument, USA) instrument in air atmosphere over a temperature range from 30 to 800 °C at a heating rate of 10 °C/min. Raman spectroscopy was performed using 785 nm laser excitation (model SDL-8530, SDL Inc.) on Reinshaw inVia Raman microscope system. FT-IR measurements were taken for raw, oxidized MWNT, and MWNT−OPH. The samples were ground with potassium bromide (KBr) to form a very fine powder using a mortar and pestle. This powder was then compressed into a thin and transparent pellet and was placed into the sample holder for analysis. Analysis was performed using a Shimadzu (Thermo-Electron Corp., Waltham, MA) bench machine with 32 scans. A drop of MWNT−OPH solution was placed on the glass slide, allowed to spread uniformly, and dried overnight. The slide was examined by field emission scanning electron microscopy equipped with an energy dispersive X-ray analyzer (JEOL USA, Inc., Peabody, MA).

Cyclic voltammetric and amperometric measurements were performed using an electrochemical analyzer CHI 660 (CH Instruments, Austin, TX) connected to a personal computer. A three-electrode configuration was employed, consisting of modified/glassy carbon (GC) electrode (3-mm diameter) serving as a working electrode, whereas Ag/AgCl (3 M KCl) and platinum wire served as the reference and counter electrodes respectively. Batch electrochemical experiments were carried out in a 2 mL voltammetric cell at room temperature (25 °C).

Oxidation of MWNTs. MWNTs were oxidized by acid treatment using one of the standard literature methods.[43,44] Briefly, raw MWNTs (100 mg) were suspended in 400 mL of concentrated H_2SO_4:HNO_3 (3:1, *v*/*v*) and sonicated in an ultrasonication bath for 6 h. The nanotube suspension was filtered through a 200 nm polycarbonate membrane and washed with Milli-Q water until pH of the solution reached ~6.5; the resulting material was dried in a vacuum oven at 80 °C for 1 day.

Enzyme Immobilization. Enzyme immobilization on carboxylated MWNTs was performed using carbodiimide chemistry. A dispersed solution that was optically homogeneous to the naked eye was obtained by mixing 2 mg of MWNT in 5 mL of deionized water and sonicating the mixture for 1 h. A total of 1 mL of MES buffer (50 mM, pH 6.2) and an equal volume of 400 mM NHS was added to the above prepared MWNT solution. EDC (20 mM) was then added to initiate the coupling of NHS to the carboxylic groups on the oxidized nanotubes and the mixture was stirred at 400 rpm for 30 min. The activated nanotube solution was then

(29) Tasis, D.; Tagmatarchis, N.; Bianco, A.; Prato, M. *Chem. Rev.* **2006**, *106*, 1105–1136.
(30) Balasubramanian, K.; Burghard, M. *Small* **2005**, *1*, 180–192.
(31) Sun, Y.; Fu, K.; Lin, Y.; Huang, W. *Acc. Chem. Res.* **2002**, *35*, 1096–1104.
(32) Chen, R. J.; Zhang, Y.; Wang, D.; Dai, H. *J. Am. Chem. Soc.* **2001**, *123*, 3838–3839.
(33) Tsai, T. W.; Heckert, G; Neves, L. F.; Tan, Y.; Kao, D. Y.; Harrison, R. G.; Resasco, D. E.; Schmidtke, D. W. *Anal. Chem.* **2009**, *81*, 7917–7925.
(34) Olek, M.; Ostrander, J.; Jurga, S.; Mohwald, H.; Kotov, N.; Kempa, K.; Giersig, M. *Nano Lett.* **2004**, *4*, 1889–1895.
(35) Nepal, D.; Balasubramanian, S.; Simonian, A. L.; Davis, V. A. *Nano Lett.* **2008**, *8*, 1896–1901.
(36) Zucolotto, V.; Pinto, A. P. A.; Tumolo, T.; Moraes, M. L.; Baptista, M. S.; Riul, A.; Araujo, A. P. U.; Oliveira, O. N., Jr. *Biosens. Bioelectron.* **2006**, *21*, 1320–1326.
(37) Zucolotto, V.; Daghastanli, K. R. P.; Hayasaka, C. O.; Riul, A.; Ciancaglini, P.; Oliveira, O. N., Jr. *Anal. Chem.* **2007**, *79*, 2163–2167.
(38) Lvov, Y.; Decher, G.; Sukhorukov, G. *Macromolecules* **1993**, *26*, 5396–5399.
(39) Crespilho, F. N.; Huguenin, F.; Zucolotto, V.; Olivi, P.; Nart, F. C.; Oliveira, O. N., Jr. *Electrochem. Commun.* **2006**, *8*, 348–352.
(40) Zucolotto, V.; Ferreira, M.; Cordeiro, M. R.; Constantino, C. J. L.; Balogh, D. T.; Zanatta, A. R.; Moreira, W. C.; Oliveira, O. N., Jr. *J. Phys.Chem. B* **2003**, *107*, 3733–3737.
(41) Crespilho, F. N.; Zucolotto, V.; Brett, C. M. A.; Oliveira, O. N., Jr.; Nart, F. C. *J. Phys. Chem. B* **2006**, *110*, 17478–17483.
(42) Dumas, D. P.; Wild, J. R.; Raushel, F. M. *J. Biol. Chem.* **1989**, *264*, 19659–19665.
(43) Li, Y.; Zhang, X.; Luo, J.; Huang, W.; Cheng, J.; Luo, Z.; Li, T.; Liu, F.; Xu, G.; Ke, X.; Li, L.; Geise, H. J. *Nanotechnology* **2004**, *15*, 1645–1649.
(44) Pedrosa, V. A.; Paliwal, S.; Balasubramanian, S.; Nepal, D.; Davis, V. A.; Wild, J.; Ramanculov, E.; Simonian, A. L. *Colloids Surf., B* **2010**, *77*, 69–74.

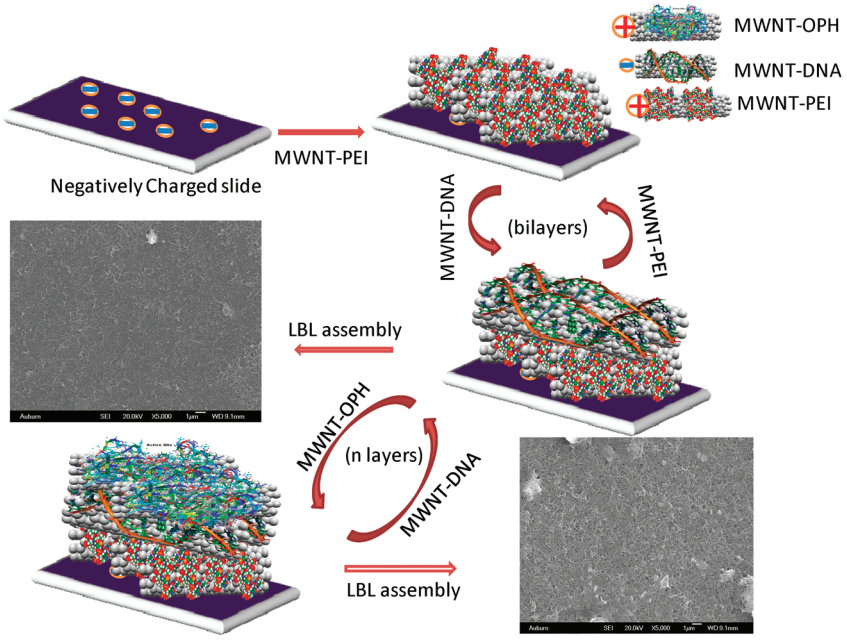

Figure 1. LbL interface design: The initial layers of MWNT−PEI and MWNT−DNA (four bilayers as shown in SEM) provide support for subsequent layers of MWNT−OPH and MWNT−DNA (nine bilayers are shown in SEM).

filtered through a 200 nm polycarbonate membrane and rinsed thoroughly with MES buffer to remove excess EDC and NHS.[44] The activated carbon nanotubes were then redispersed in 9.0 mL of MES buffer solution and 1.0 mL of a 0.2 mg/mL OPH in 20 mM CHES buffer solution, pH 9.0. After incubating the mixture on a platform shaker at 4 °C for 9.5 h, the nanotube suspension was centrifuged (13,200 rpm, 30 min each) and rinsed with MES buffer solution three times to remove unbound protein. The protein−nanotube conjugate was finally suspended in CHES buffer solution.

Oxidized MWNTs were separately dispersed in PEI (1 mg/mL) by tip sonication using a standard 13 mm probe. Heating was minimized through the use of a water bath. The excess polymer was then removed by centrifugation at 13,200 rpm for about 30 min. A dispersion of 0.1 wt % of DNA was prepared using our previously published method for individual SWNT dispersion.[35] DNA was dissolved in water at 35 °C for about 45 min using a magnetic bar. 0.1 wt % of MWNT was dispersed in the aqueous DNA by tip sonication for 1 h; an ice water bath was used for cooling. The resulting dispersion was centrifuged at 13,200 rpm for about 30 min to remove aggregates and reduce the amount of unbound DNA.

Layer-by-Layer Assembly of MWNT Thin Films. Glass or silicon slides were cleaned in concentrated H_2SO_4/30% H_2O_2 (3:1) ("piranha" solution; **caution must be taken as the piranha solution readily causes chemical burns and is highly reactive, particularly with organic materials**) to remove contaminants and to form a negatively charged surface, followed by copious rinsing with ultrapure water. The negatively charged slides were alternately immersed in aqueous dispersion of MWNT−PEI and MWNT−DNA. The adsorption time of 15 min was considered sufficient for the formation of MWNT monolayer. After each layer's deposition, the substrate was rapidly dried using 50 psi air from a nozzle for 30 s. On top of these cushioning layers, alternate layers of MWNT−OPH and MWNT−DNA were deposited by immersing the slide in aqueous solutions of MWNT−OPH and MWNT−DNA for 15 min. The surface was renewed by immersing the slides in MWNT−OPH solution for 15 min. These solutions appear stable even after a year.

Layer-by-Layer Assembly of MWNT Thin Films on Glassy Carbon Electrode. The glassy carbon electrode (GCE) was polished with 0.10 and 0.05 μm alumina slurries and then ultrasonically cleaned in water for 15 min. The GCE electrode was immersed in a 1 M NaOH solution for 5 min and a 1.2 V potential was applied to introduce negative charges on the surface; this was followed by two washings steps with distilled water. The positively charged MWNT−PEI was adsorbed by dipping the negatively charged GC electrode in an aqueous solution of MWNT−PEI for 15 min, and the MWNT−PEI/GC electrode was dried under nitrogen. Using the same procedure, a layer of negatively charged MWNT−DNA was adsorbed. Following that, a MWNT−OPH layer was adsorbed on the $(MWNT-DNA/MWNT-PEI)_4$/GC electrode by dipping into the MWNT−OPH solution; additional bilayers were formed in the same way. The modified electrode was stored at refrigerated conditions until use. All of the electrochemical measurements were performed at room temperature. A three electrode system containing platinum as auxiliary electrode, an LbL modified glassy carbon working electrode, and a saturated Ag/AgCl reference electrode was used. The buffer solution was 50 mM PBS (pH 7.54). The regeneration of the biosensor interface was realized by immersing the sensor in a fresh solution of MWNT−OPH for 15 min.

Results and Discussion

Structural Characterization. Thermogravimetric analysis (TGA) was carried out to assess the mass of functional groups on the surface of nanotubes (Figure 2). The presence of functional groups in the oxidized MWNTs resulted in increased weight loss relative to raw MWNTs upon heating from 200−550 °C; this is due to the decomposition of functional groups such as carboxyl and hydroxyl groups at high temperature.[45] For the raw MWNT sample, the significant weight loss starts at ~400 °C and ends at ~550 °C. Weight losses in this temperature range were 13% and 1% for oxidized MWNT and raw MWNT, respectively. This result validates the effective functionalization on the nanotube surfaces during the acid treatment.

Further confirmation of nanotube functionalization was provided by Raman spectroscopy. Measuring relative intensities of the Raman D and G bands, emanating from the tangential stretching modes of the sp^3 hybridized and sp^2-hybridized carbons, respectively is a commonly employed tool for detecting covalent bond

(45) Li, Z.; Ni, Q. Q.; Fu, Y.; Natsuki, T. *Appl. Surf. Sci.* **2009**, *255*, 7095–7099.

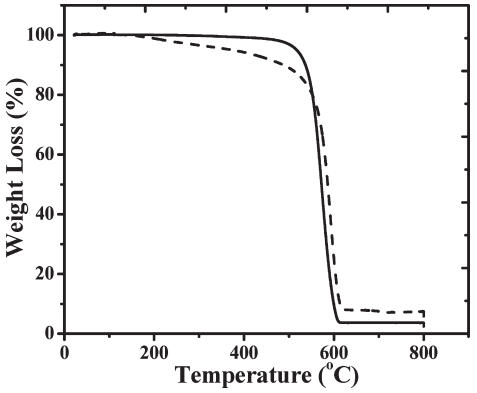

Figure 2. TGA analysis of intact MWNT(—) and oxidized MWNT (---) in air atmosphere.

formation in CNTs.[46,47] Figure 3a shows the intensities of these characteristic peaks, namely, the D band at 1305 cm^{-1} and the G band at 1580 cm^{-1}. The D/G ratios of raw MWNTs and oxidized MWNTs were around 1.36 and 1.7, respectively, confirming an increased degree of functionalization.[43,44] SEM also shows that the functionalized MWNTs were sufficiently dispersed to produce a layer after attachment of the biopolymer. For example, Figure 3c shows an image of MWNT−OPH. It exhibits a high-density of MWNTs; the initial oxidized dispersion consisted of MWNTs bundles on the order of 5 nm in diameter. In order to get direct affirmation for the added functional groups on the nanotube surfaces and immobilization of OPH on oxidized MWNT, FT-IR analysis was performed on raw MWNT, oxidized MWNT, and MWNT−OPH samples.

Figure 3b shows spectra of raw MWNT, oxidized MWNT, and MWNT−OPH. The oxidation of MWNTs by the combination of H_2SO_4 and HNO_3 results in the formation of hydrophilic groups at defect sides and ends, −COOH and −OH.[48] All spectra for the oxidized MWNTs displayed a peak at 1737 cm^{-1} corresponding to the C═O stretching mode of the carboxylic acid. These results are consistent with previous work on CNT oxidation; the exact peak positions are the result of the extent of oxidation.[49] In addition, the increased intensity of the 3434 cm^{-1} peak suggests introduction of more −OH groups after acid treatment.[11] However, after the enzyme immobilization on oxidized MWNT, the 1737 cm^{-1} peak disappeared and a new peak at ~1634 cm^{-1} was observed. This can be attributed to the in-plane N−H molecular vibrations of the amine group. It is believed that a substitution reaction occurs and a −NH group replaces the −OH group of the carboxylated MWNTs after amide functionalization to form the −CO−NH functional group.[44]

UV−Vis Absorption Studies. It is well-known that OPH hydrolyzes the phosphotriester bond of the model OP paraoxon (λ_{max} = 274 nm), releasing the hydrolysis product p-nitrophenol (PNP) (λ_{max} = 405 nm).[42] Thus, UV−vis spectroscopy can be used to confirm successful immobilization of OPH and observe selective hydrolysis of paraoxon to PNP. Absorption spectra showed two peaks, one corresponding to paraoxon at 274 nm and a peak at 405 nm corresponding to PNP (Figure 4). Presumably, the activity of layers with catalytically active biopolymer should be different from that for noncatalytic layers. Slides with different numbers of layers ending with MWNT−OPH (odd

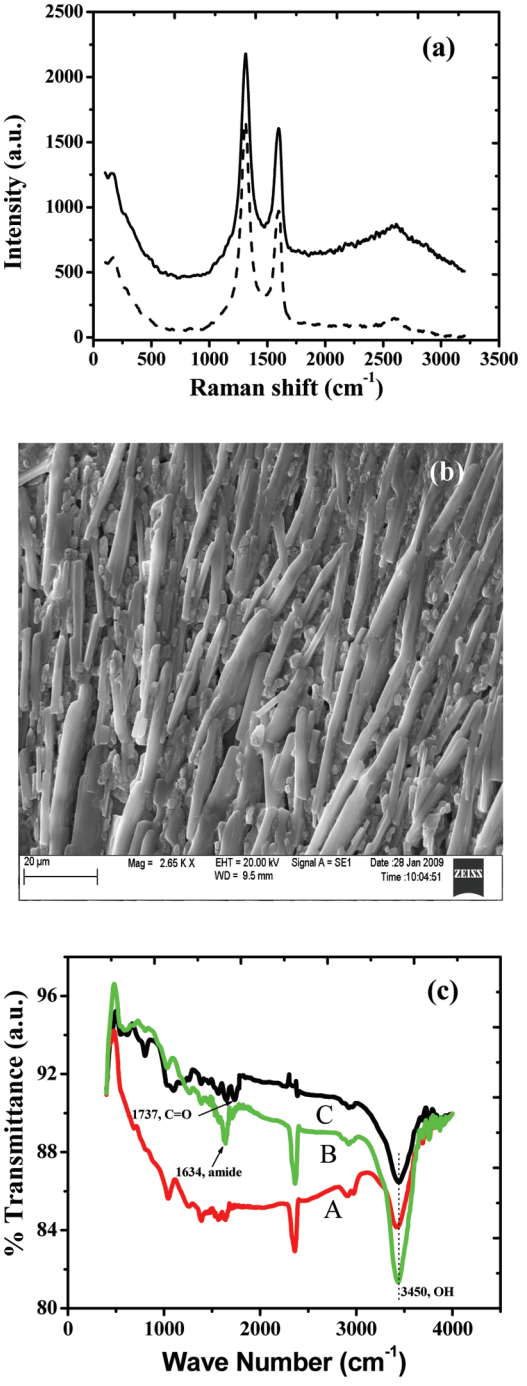

Figure 3. (a) Raman spectra of raw MWNT (—) and oxidized MWMT (---) using 785 nm laser; (b) SEM image of MWNT-OPH on glass slide; (c) FT-IR spectra of (A) raw MWNT, (B) MWNT-OPH and (C) oxidized MWNT.

layers) or MWNT−DNA (even layers) were exposed to 0.1 μM paraoxon for 10 min and the absorption spectrum was recorded. As shown in the Figure 4 inset, the absorption at 405 nm increased with the number of layers for surfaces ending in MWNT−OPH, indicating changes in the enzymatic activity proportional to the number of enzyme layers. In contrast, the absorbance was much lower for even layers ending with MWNT−DNA. These results indicate that assembled multilayers are relatively permeable for paraoxon, which penetrate into the deeper layers and react with OPH. More detailed investigation of layer density and the depth of substrate penetration and permeability in such interfaces is the subject of further investigations.

(46) Graupner, R. *J. Raman Spectrosc.* **2007**, *38*, 673–683.
(47) Hayden, H.; Gunko, Y. K.; Perova, T. S. *Chem. Phys. Lett.* **2007**, *435*, 84–89.
(48) Orbulescu, J.; Constantine, C. A.; Rastogi, V. K.; Shah, S. S.; DeFrank, J. J.; Leblanc, R. M. *Anal. Chem.* **2006**, *78*, 7016–7021.
(49) Bahr, J. L.; Tour, J. M. *J. Mater. Chem.* **2002**, *12*, 1952–1958.

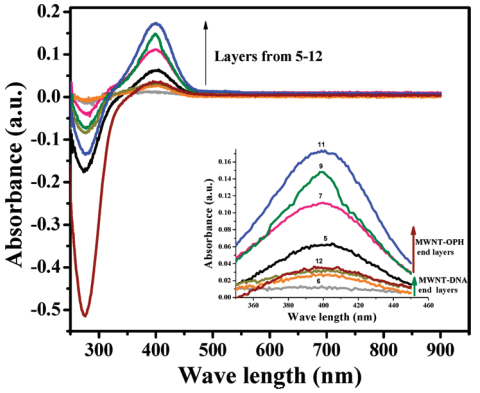

Figure 4. UV−vis absorption spectra of LbL assembly for different number of layers by exposing the surface to 0.1 mM Paraoxon for 10 min. Odd layers are ending with MWNT−OPH.

Electrochemical Activity of Multilayer Films. The catalytic activity of the LbL assembled MWNT−OPH interface was also characterized electrochemically on the glassy carbon (GC) electrode. To characterize the impact of the number of active layers at the interface, films terminating in MWNT−OPH with 5−11 bilayers were investigated. Cyclic voltammetry (CV) shows that the anodic peak currents (i_{pa}) are linearly proportional to the square root of scan rates (Figure 5a inset), revealing that the electrocatalytic oxidation of PNP is a diffusion-controlled process.[50,51] As expected, modified electrode film (Figure 5b) shows an oxidation peak at 0.90 V. The oxidation peak of PNP electro-oxidation current increases linearly with increasing number of active layers (Figure 5b inset). For the layers ending with MWNT−OPH current response gradually increases up to 9 layers and saturates with 11 layers. A possible explanation for this phenomenon is that the distance between the 11th layer and the electrode is great enough to diminish the electron communication.[52] Additionally, such saturation can be attributed to the diffusion control due to the limited access to the deeper layers. For the layers ending with MWNT−DNA a much lower response was observed, in accordance with previous absorption studies. These results indicate that each MWNT−DNA only partially hinders the paraoxon accessibility to the next active layer so that we are observing reducing activity with increasing numbers of bilayers. The observed saturation of the signal indicates diminishing contribution of lower OPH layers.

Figure 6a shows flow-injection calibration data for paraoxon over the concentration range of 0.5−10 μM, and the inset shows that current linearly increased with the concentration in the range from 0 to 10 μM. The system showed excellent sensitivities ($y = -8 \times 10^{-10} + 0.074\ \mu A\ \mu M^{-1}\ cm^{-2}$ calculated from the slopes of the linear part of the calibration curve). In addition, based on an estimated signal-to-noise (S/N) ratio of 3, the sensor has a detection limit of 77 nM paraoxon. As shown in Table 1 the biosensor is demonstrating both a higher sensitivity and lower detection limit than achieved in previous works. These results are due to the combination of the large specific surface area enabled by the oxidized MWNT dispersion, and favorable interactions between the MWNTs and OPH and within each layer. Assembly of MWNTs can provide a favorable biocompatible microenvironment for maintaining enzymatic activity. This may be due to the favorable situation

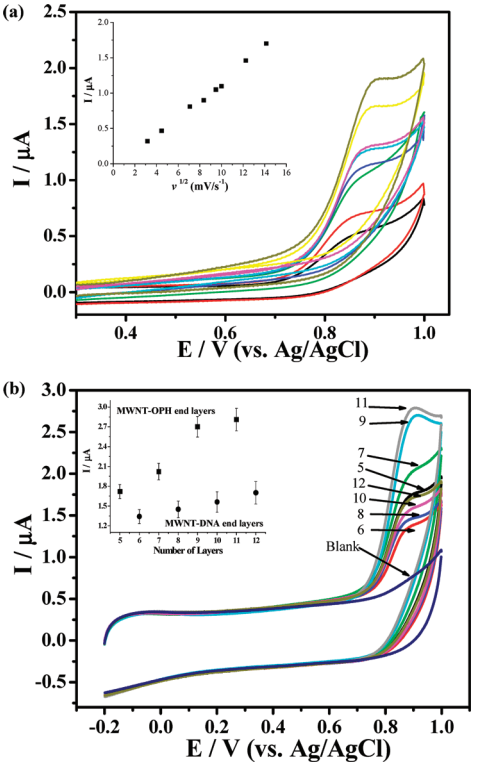

Figure 5. (a) CV response of five layers (ending with MWNT−OPH) using various scan rates 10, 20, 50, 70, 90, 100, 150, and 200 mV/s in 10 mM of PBS in the presence of 10 μM Paraoxon. Inset CV shows anodic current vs square root of scan rate. (b) CV response using LbL assembly for different number of layers (odds ending with MWNT−OPH and evens ended with MWNT−DNA). Inset: Correlation of current at 0.90 V vs number of layers (maximum peak current corresponding to PNP oxidation potential).

with low transport limitations of substrate, which are a result of the special spatial distribution of the MWNT-immobilized enzymes and leads to the better accessibility of the substrate molecules.

Long-Term Stability Analysis. Figure 6b shows the sensor response for a 2 μM concentration of paraoxon. When the biosensor was not in use, it was stored in buffer at 4 °C. The current response decreased slightly in the initial few days, and afterward the response tended to be nearly constant and retained 85% of its original response over two months of storage. The response dropped to 45% of the initial signal after 6 months. However, because of kinetic mode operation, this biosensor can be easily calibrated during all operational time. The significant reduction of the initial activity is not a problem since the slope of calibration curve is steep enough to provide appropriate parameters of the sensor and reliable detection. The RSD (relative standard deviation) is 6.0% estimated from slopes of calibration plots for five different and freshly prepared electrodes, revealing an acceptable repeatability in the construction of the electrode.

Surface Regeneration Studies. Since the catalytic activity of the interface decreases with time, it is desirable to regenerate it after significant reduction of the activity.[53] The electrode surface was renewed after 6 months of usage, when the electrode response dropped to 45% of its original value. As shown in Figures 6b and 7, we discovered that immersing the electrode in the MWNT−OPH solution for 15 min is a very easy way to

(50) Yan, X. B.; Chen, X. J.; Tay, B. K.; Khor, K. A. *Electrochem. Commun.* **2007**, *9*, 1269–1275.
(51) Zhu, C.; Guo, S.; Zhai, Y.; Dong, S. *Langmuir* **2010**, *26*, 7614–7618.
(52) Zhang, W.; Huang, Y.; Dai, H.; Wang, X.; Fan, C.; Li, G. *Anal. Biochem.* **2004**, *329*, 85–90.
(53) Pedrosa, V. A.; Caetano, J.; Machado, S. A. S.; Freire, R. S.; Bertotti, M. *Electroanalysis* **2007**, *19*, 1415–1420.

Table 1. Comparison of Analytical Performance of Some Paraoxon Biosensors

Paraoxon biosensor	sensitivity	limit of detection (μM)	ref
MWNT−OPH/MWNT−DNA	0.074 μA μM^{-1} cm^{-2}	77.0×10^{-3}	
MWNT/OPH	25 nA μM^{-1}	800.0×10^{-3}	54
PNP-degrader *Pseudomonas putida* JS444 expressing organophosphorus hydrolase	0.31 Δ% O_2 μM^{-1}	0.20	55
fluorescence probe		160.0	56
screen-printed electrode coupled with choline oxidase	5.03 μA mM^{-1} cm^{-2}	0.10	57
physical entrapment AChE−AuNPs−SiSG		2.69	58

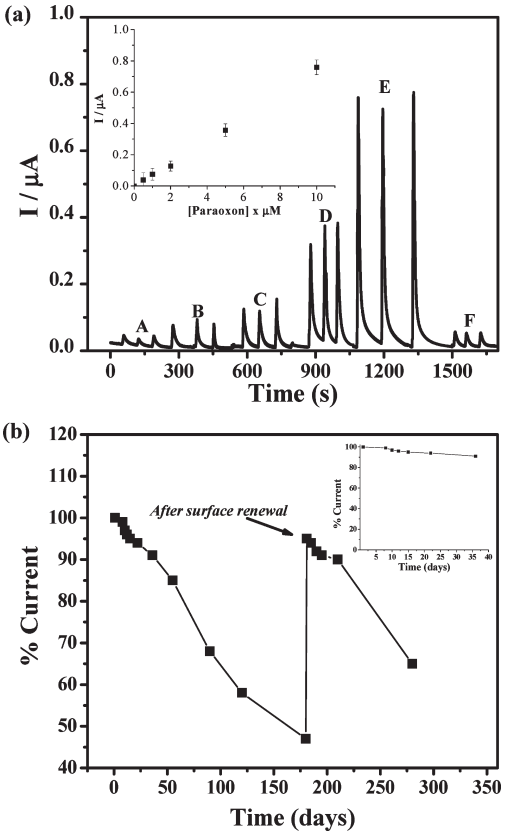

Figure 6. (a) Flow-injection analysis on LbL modified electrode (five layers ending with MWNT−OPH) by sequential injection of Paraoxon: (A) 0.5, (B) 1.0, (C) 2.0, (D) 5.0, (E) 10.0, and (F) 0.5 μM. Inset: Calibration curve. (b) Long-term stability of the sensor for 2 μM concentration of paraoxon. Inset: Response changes during 35 days.

restore up to 95% of the original response level. This outstanding result can be explained in the following manner. The gradually reducing activity of the electrode with time is most likely due to depletion of the top MWNT−OPH. The activity of the surfaces ending with MWNT−DNA are about 50% less than for those ending with MWNT−OPH (Figure 5b inset), we therefore believe that after 6 months of use the electrode surface has completely lost its MWNT−OPH upper layer (Figure 6b) and the negatively charged MWNT−DNA layer is exposed to the solution. Therefore, immersing the electrode in the MWNT−OPH solution allows redeposition of an active MWNT−OPH layer and restoration of initial activity. Thus, this simple procedure of interface reactivation brings a significant advantage of the LbL assembly over other technologies and allows using the biosensor for very long time.

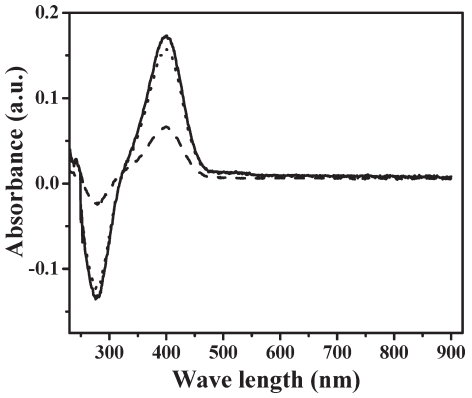

Figure 7. UV−vis absorption spectra for 11 layers of LbL assembly. The solid line is for freshly prepared slide; the dashed line presents activity after 6 months, and the dotted line is for the renewal surface. For renewal the surface was immersed in MWNT−OPH solution for 15 min, and the paraoxon concentration was 0.1 mM.

Conclusions

In conclusion, this approach to the generation of multifunctional LbL biopolymer nanocomposite interfaces with distinct structures and properties is relatively simple, does not require complex synthesis, and yields excellent catalytically active interfaces appropriate for biosensing and other applications. Each adsorbed layer can be used as an anchoring surface for the next subsequent functional layer. To demonstrate this ability, alternate layers of MWNT−DNA and OPH immobilized on MWNTs were successfully adsorbed onto functionalized carbon nanotube surfaces with four PEI−DNA cushioning bilayers and were used for sensitive detection of paraoxon. These sturdy and stable ultrathin nanocomposite films provide a scaffold for the biopolymers with capability to preserve catalytic activity of the proteins for a long time and also can be easily regenerated. This in turn is an excellent opportunity to use such nanofunctionalized materials in biosensing and biomimetic applications.

Acknowledgment. This research was supported by grants from the National Science Foundation (CAREER CMMI-0846629) and NIFA (2006-34394-16953). The work reported herein was also performed under USAF SG-approved Clinical Investigation FDG20060049N, FKE20090002E, and USAF CRADA 07-277-60MDG-01. Additionally, this material was based on work which supported A.L.S. by the National Science Foundation, while working at the Foundation. This work could not be accomplished without OPH, generously provided from Dr. J. Wild's Laboratory at TAMU.

(54) Deo, R. P.; Wang, J.; Block, I.; Mulchandani, A. P.; Joshi, K. A.; Trojanowicz, M.; Scholz, F.; Chen, W.; Lin, Y. *Anal. Chem. Acta* **2005**, *530*, 185–189.
(55) Lei, Y.; Mulchandani, A. P.; Chen, W. *J. Agric. Food Chem.* **2005**, *53*, 524–527.
(56) Jin, S.; Xu, Z.; Chen, J.; Liang, X.; Wu, Y.; Qian, X. *Anal. Chem. Acta* **2004**, *523*, 117–123.
(57) Sajjadi, S.; Ghourchian, H.; Tavakoli, H. *Biosens. Bioelectron.* **2009**, *24*, 2509–2514.
(58) Du, D.; Chen, S.; Cai, J.; Zhang, A. *Biosens. Bioelectron.* **2007**, *23*, 130–134.